Effect of Al metal precursor on the phase formation and mechanical properties of fine-grained SiAlON ceramics prepared by spark plasma sintering

Moath Mohammad Al Malki [a], Raja Muhammad Awais Khan [b], Abbas Saeed Hakeem [c,*], Stuart Hampshire [d], Tahar Laoui [a,c,*]

[a] Mechanical Engineering Department, King Fahd University of Petroleum & Minerals, Dhahran 31261, Saudi Arabia
[b] College of Aeronautical Engineering, National University of Science & Technology (NUST), Pakistan
[c] Center of Excellence in Nanotechnology, King Fahd University of Petroleum & Minerals, Dhahran 31261, Saudi Arabia
[d] Materials and Surface Science Institute, University of Limerick, Limerick, Ireland

ARTICLE INFO

ABSTRACT

This paper reports the effects of using nano-precursor powders, including α-Si$_3$N$_4$ or amorphous-Si$_3$N$_4$, and particularly the partial replacement of AlN by Al metal precursor, on the properties of a fixed Ca-α-SiAlON composition, consolidated by spark plasma sintering at 1450 °C and 1600 °C. The observed changes in mechanical properties are related to the phases present in the microstructures. In addition to allowing the consolidation of dense and fine ceramics at lower temperatures, the partial replacement of AlN by Al metal precursor has shown remarkable improvement in the mechanical properties of samples sintered at 1600 °C containing α-Si$_3$N$_4$, a result of fine α-SiAlON grains and nitrogen-rich grain boundary phase. Another key contribution of Al metal precursor is found in lowering the sintering temperature while keeping, or even improving, the mechanical properties of the sintered samples, as observed in samples sintered at 1450 °C.

© 2016 Elsevier Ltd. All rights reserved.

1. Introduction

SiAlONs are solid solutions based on the α- and β- silicon nitride structures, in which part of the Si and N is replaced by Al and O, respectively, in order to maintain charge neutrality [1–4]. Based on the starting composition and the sintering parameters, several phases can be formed including: α-SiAlON [2,3], β-SiAlON [1,4,5], O'-SiAlON [4], X-SiAlON [4,6] or mixtures of these [6–8]. In particular, α- and β- SiAlONs have attracted much attention in the past two decades due to their exceptional mechanical properties, namely high hardness for α-SiAlON and reasonable fracture toughness for β-SiAlON [9,10].

α-SiAlONs are based on the α-Si$_{12}$N$_{16}$ unit cell with stoichiometric formula [2]: $M_xSi_{12-(m+n)}Ai_{(m+n)}O_nN_{16-n}$ where m is the number of Al—N bonds, n is the number of Al—O bonds, M represents the added cation, such as many of the rare earth lanthanides and alkaline earth elements, $x = m/v \leq 2$ where v indicates the valence of the added cation. α-SiAlON is formed from the reaction of silicon nitride, aluminum nitride and the oxide of the appropriate modifying cation M (Y$_2$O$_3$, CaO, etc.) and, as with silicon nitride and β-SiAlONs, densification occurs by liquid phase sintering.

Generally, α-SiAlON possesses higher hardness than β-SiAlON, while the latter shows better fracture toughness than the former. The reason behind this variation in the mechanical properties is explained usually through the consideration of the phase morphologies, in which α-SiAlON is formed mainly as equiaxed grains, while β-SiAlON grains tend to be elongated hexagonal prisms. However, scientists have successfully developed ceramics with elongated α-SiAlON grains to enhance fracture toughness [11,12].

Lanthanide sintering additives, such as the oxides of Nd, La and Yb, have been predominantly the major research interest in the last decade [13–16]. However, because of the relatively high cost of these rare earths [17], the research focus has shifted to other

* Corresponding authors at: Mechanical Engineering Department and Center of Excellence in Nanotechnology, King Fahd University of Petroleum & Minerals, Dhahran 31261, Saudi Arabia

E-mail addresses: mmalki@kfupm.edu.sa (M.M. Al Malki), rawais@cae.nust.edu.pk (R.M.A. Khan), ashakeem@kfupm.edu.sa (A.S. Hakeem), stuart.hampshire@ul.ie (S. Hampshire), tlaoui@kfupm.edu.sa (T. Laoui).

Table 1
Chemical powder reactants in wt.%.

Sample Name	CaO	Al_2O_3	α-Si_3N_4	Amp-Si_3N_4	AlN	Al	N[a]
α(0Al)	9.31	16.92	46.56	–	27.21	–	–
α(0.1Al)	9.31	16.92	46.56	–	24.49	1.79	0.93
α(0.2Al)	9.31	16.92	46.56	–	21.77	3.58	1.86
α(0.3Al)	9.31	16.92	46.56	–	19.05	5.37	2.79
Amp(0Al)	9.31	16.92	–	46.56	27.21	–	–
Amp(0.1Al)	9.31	16.92	–	46.56	24.49	1.79	0.93
Amp(0.2Al)	9.31	16.92	–	46.56	21.77	3.58	1.86
Amp(0.3Al)	9.31	16.92	–	46.56	19.05	5.37	2.79

[a] Assuming stoichiometric reaction: $Al + 1/2N_2$ (gas) $\rightarrow$ AlN.

additives, such as alkaline earth elements, namely Ba, Mg and Ca. Among the aforementioned elements, Ca seems to be the promising candidate to replace many of the lanthanide additives as it can be incorporated easily into the α-SiAlON structure without any notable crystal distortion [18–20]. Further, it is readily available from many mineral precursors including fly ash, which explains the relative low price of Ca compounds compared with other alternatives [21].

Over the last few years, researchers have utilized spark plasma sintering (SPS) as a consolidation technique for various powder mixtures to form ceramics. Compared to other sintering techniques, the heating rate is very high and also due to the pulsed nature of the current, SPS has confirmed its benefits of rapidly densifying compacted powders at relatively low temperatures [22–24]. Various types of silicon nitride based ceramics, including α-SiAlON, can be sintered to full density by the SPS process at lower temperatures and with substantially shorter holding times than conventional processes. The phase assemblages, however, may be far from equilibrium due to the very fast consolidation taking place in SPS [25].

One aim of the present work was to investigate the effect of Al metal precursor on the densification and mechanical properties of Ca-α-SiAlON ceramics using SPS. The idea of metal precursors has been introduced before by Hakeem et al. [26], but in the context of synthesizing high N content oxynitride glasses. It is expected that the use of such a metal precursor will aid electrical conductivity in the early stages of SPS and in the later stages may increase the amount and mobility of the liquid phase and, thus, the ceramic densification. A further aim was to compare crystalline and amorphous Si_3N_4 starting powders in order to study the impact of the structure on the densification and mechanical properties. Samples were sintered by the SPS process to achieve the highest possible densification in the shortest time due to the high heating rate.

2. Experimental procedure

The chemical composition was fixed to be: $CaSi_6Al_6O_4N_{12}$ which corresponds to m = 2 and n = 4 in the general formula for α-SiAlON and was made up using only AlN or replacement of 10, 20, and 30 mol% of Al in AlN by Al metal. Although Ca-α-SiAlONs usually have a limit of Al and O solubility lower [2,3] than in this composition, the composition was chosen to allow excess liquid formation and to assess how (1) the use of different silicon nitride powders, (2) the substitution of Al metal for Al in AlN and (3) the SPS processing affects phase formation and the overall phase assemblages in order to form Ca-SiAlON nano-composites. Table 1 lists the investigated compositions with the respective proportions of the used precursors. The starting materials were either α-Si_3N_4 (250 nm – Ube Industries SN-10, Japan) or amorphous Amp-Si_3N_4 (20 nm – Chempur, Germany), plus α-Al_2O_3 (150 nm – Chempur, Germany), CaO (160 nm – Sigma Aldrich, USA) and AlN (150 nm – Sigma Aldrich, USA) with partial substitution of Al metal (44 μm – Loba Chemie, India).

The chemical reaction for a sample without Al replacement can be written as follows:

$$CaO + Al_2O_3 + 2Si_3N_4 + 4AlN \rightarrow CaSi_6Al_6O_4N_{12} \qquad (1)$$
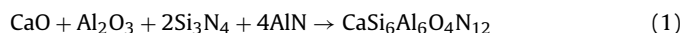
Now, if 10 mol% of AlN is substituted by Al metal, this can be represented by the following:

$$CaO + Al_2O_3 + 2Si_3N_4 + 3.6AlN + 0.4Al + 0.2N_2 \rightarrow CaSi_6Al_6O_4N_{12}$$
$$(2)$$
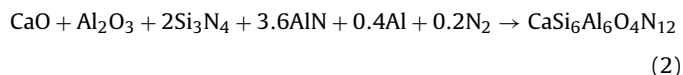
Accordingly 5 g powder samples were weighed and mixed using an ultrasonic probe sonicator for 20 min with ethanol as a mixing medium. To remove ethanol, samples were dried at 80 °C for 12 h. SPS was carried out by pouring the powder mixtures into 20 mm diameter graphite dies. Sintering was performed firstly for all samples at 1600 °C for 30 min in the presence of nitrogen, under a uniaxial load of 50 MPa. Samples containing α-Si_3N_4 were also sintered at 1450 °C, to evaluate the role of Al in enhancing sinterability at lower temperatures at which more α-SiAlON would be expected to be retained. A heating rate of 100 °C/min. was adopted in an attempt to avoid formation of intermediate phases. Samples were then rapidly cooled down to ambient temperature.

SPSed samples were cleaned of graphite using SiC grinding papers (120 grit size), followed by additional diamond disc grinding to remove the graphite paper and prepare clear surface for density measurement. Later, automatic grinding and polishing machine (Automet 300 Buehler grinding machine) was utilized to prepare samples for subsequent microstructural and mechanical investigations. The grinding process included the use of diamond wheels (74 μm, 40 μm, 20 μm, 10 μm particle size), followed by the use of diamond suspensions (9 μm, 6 μm, 3 μm, 1 μm, 0.25 μm) in the polishing stage. A Rigaku MiniFlex X-ray diffractometer (Japan) was used to identify phases present in the synthesized samples, using Cu K$_{\alpha 1}$ radiation (γ = 0.15416 nm), accelerating voltage = 30 kV and tube current = 10 mA. Samples were then gold-coated in a sputter coating machine (108 Auto Sputter Coater, TED PELLA) for very short time to deposit approximately 10 nm coating thickness. Afterwards, samples were examined under a field emission scanning electron microscope (FESEM, Lyra 3, Tescan, Czech Republic) using both secondary electron (SE) and back-scattered electron (BSE) detectors, with accelerating voltages of 20–30 kV in order to characterize grain morphologies, and an energy dispersive X-ray spectroscope (EDX, Oxford Inc., UK) was used for elemental analysis of the phases present. Particles size analyzer (Turbotrac Model S3500, Microtrac) was used to evaluate the powder size for certain precursors. Density was measured based on an Archimedes method. Vickers hardness (10 kg load) was evaluated using a universal hardness tester (Zwick-Roell, ZHU250, Germany). The facture toughness was obtained using the indentation method, utilizing Evan's formula [27]:

$$K_{IC} = 0.48 \left(\frac{MCL}{d/2} \right)^{-1.5} \left(\frac{HV_{10}\sqrt{d/2}}{3} \right)$$

An average of 8–10 readings per sample were taken to evaluate both Vickers hardness and indentation fracture toughness, covering different phases in the microstructures of the investigated samples. The hardness and fracture toughness values should be considered only as good estimates to carry out a comparative analysis between the sintered samples.
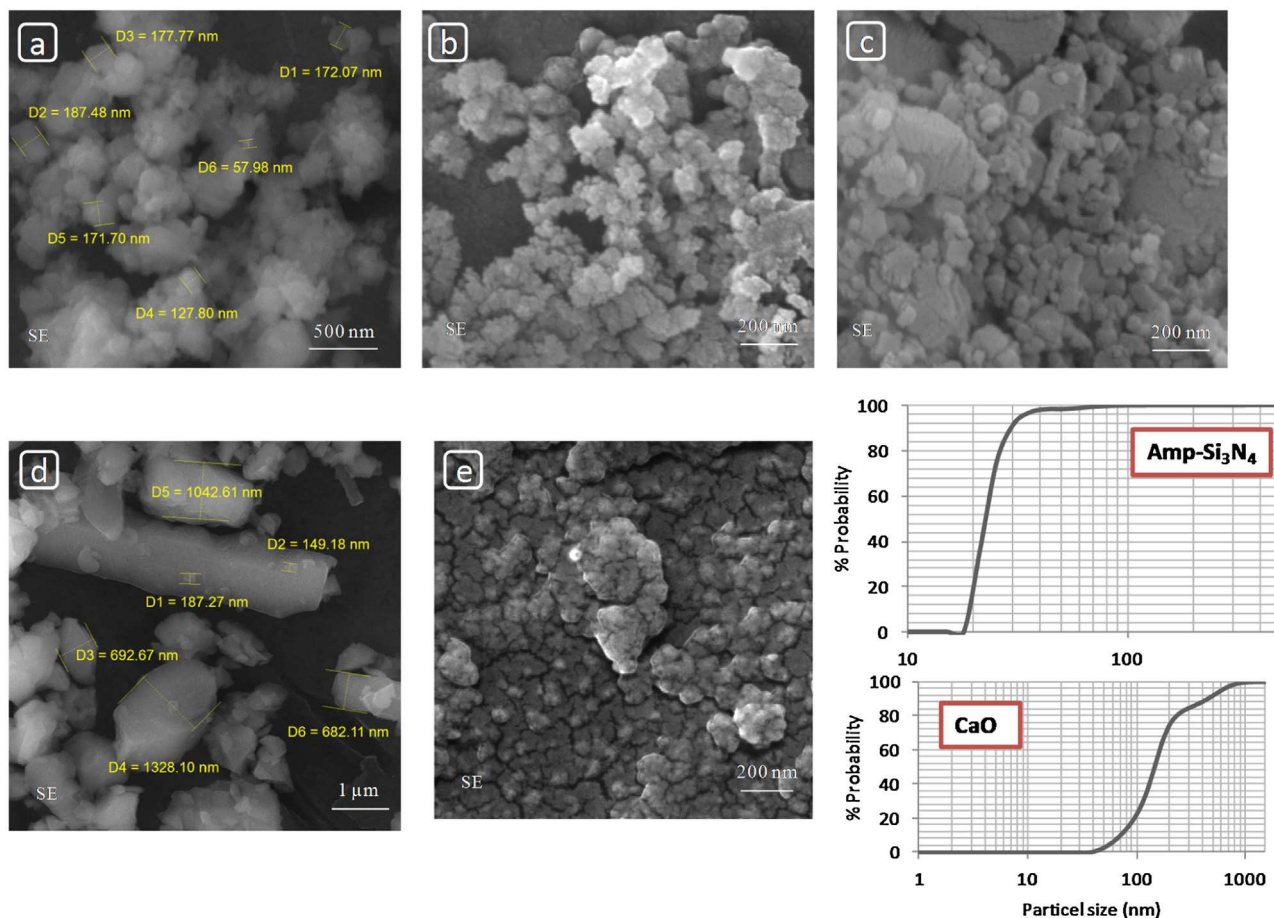
Fig. 1. SEM micrographs of the starting powders. (a) α-Si$_3$N$_4$, (b) Amp-Si$_3$N$_4$, (c) CaO, (d) AlN, (e) Al$_2$O$_3$. The particle size analysis for Amp-Si$_3$N$_4$ and CaO is shown as well.
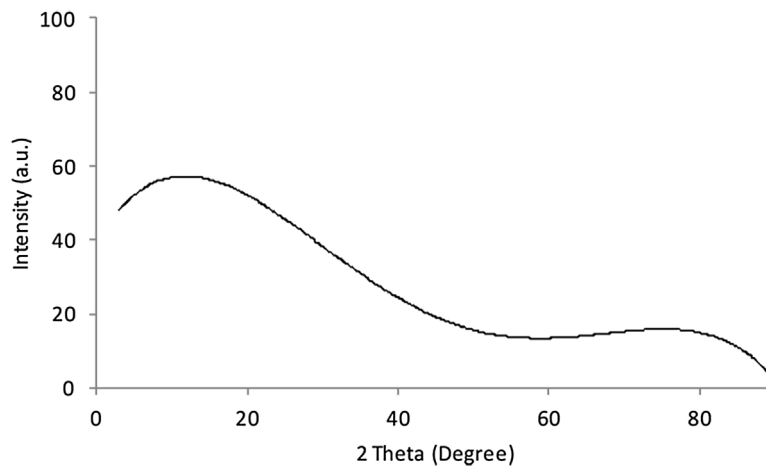

Fig. 2. XRD pattern of as-received Amp-Si$_3$N$_4$.

3. Results and discussion

3.1. Starting powders analysis

SEM micrographs of the starting powders are shown in Fig. 1. Besides, Particles size analysis results are shown for Amp-Si$_3$N$_4$ and CaO starting powders. α-Si$_3$N$_4$ particel size ranges from 150 to 250 nm, while Amp-Si$_3$N$_4$ particles hold a size of about 20–30 nm, in agreement with the data provided by the manufacturers. Similarly, AlN and Al$_2$O$_3$ particles size falls in the range 100–200 nm. The particle size analysis of CaO suggests that around 85% of the used powder holds a size equal to or below 134 nm. The X-ray diffraction pattern for Amp-Si$_3$N$_4$ starting powder is shown in Fig. 2, confirming the amorphous nature of the powder.

3.2. Sintering and densification

Table 2 shows the densities of the SiAlON ceramic samples sintered at 1600 °C and 1450 °C. All densities were ∼3.10 g cm^{-3} or above, which is close to the theoretical density of pure Ca-α-

Table 2
Density values in g/cm^3 of samples sintered at 1600 °C and 1450 °C.

	α(0Al)	α(0.1Al)	α(0.2Al)	α(0.3Al)	Amp(0Al)	Amp(0.1Al)	Amp(0.2Al)	Amp(0.3Al)
1600 °C	3.11	3.15	3.10	3.15	3.11	3.09	3.10	3.09
1450 °C	3.17	3.16	3.16	3.15	–	–	–	–

SiAlON. However, the samples have complex phase assemblages (see Section 3.3) and evaluating their theoretical densities is quite difficult, due to the fact that the density values for individual phases obtained from XRD are not known. However, it may be concluded that samples are approaching full density when compared to values obtained in the literature for similar compositions. The partial substitution of AlN with Al in the samples containing α-Si$_3$N$_4$ sintered at 1600 °C showed a very slight increase in density whereas samples containing amorphous Si$_3$N$_4$ showed no increase with Al substitution. The fact that density values did not change much through the incorporation of metallic Al may indicate that the amount of liquid phase formed remains the same and, thus, there is no difference in overall densification. It is notable that the samples containing α-Si$_3$N$_4$ sintered at 1450 °C still have the same densities as or better than those sintered at 1600 °C. This would suggest that, for these compositions, by using SPS with its inherent rapid heating rate and the associated uniaxial pressure, densification can be achieved very easily even at lower peak temperatures.

3.3. Phase assemblage

XRD patterns of samples α(0Al), α(0.1Al), α(0.2Al) and α(0.3Al) sintered at 1600 °C are shown in Fig. 3. β-SiAlON z = 3 (Si$_3$Al$_3$O$_3$N$_5$) is the major phase in sample α(0Al) along with some 15R polytypoid (SiAl$_4$O$_2$N$_4$). However, as Al metal is substituted for AlN into the starting mixture, the major phase is Ca-α-SiAlON, with a small amount of β-SiAlON and 12H polytypoid (SiAl$_5$O$_2$N$_5$). As more Al metal is added into the mixture, some of the 12H is replaced by 21R (SiAl$_6$O$_2$N$_6$) with the nitrogen to oxygen ratio of the polytypoid phase increasing. It can be noted that Si is also present in the samples containing higher amounts of Al, i.e. α(0.2Al) and α(0.3Al).

Fig. 4 presents the XRD patterns of samples Amp(0Al), 3-Amp(0.1Al), 3-Amp(0.2Al) and Amp(0.3Al) formed from nano-sized amorphous silicon nitride and sintered at 1600 °C. β-SiAlON z = 1.2 (Si$_{4.8}$Al$_{1.2}$O$_{1.2}$N$_{6.8}$) is the major phase in sample Amp(0Al) along with 12H polytypoid. When a small amount of Al is substituted for AlN in sample Amp(0.1Al) a small amount of a low substituted α-SiAlON is formed but this does not appear in the samples containing higher levels of Al. The z value of β-SiAlON increases as Al is substituted for AlN to z = 3.2 in sample Amp(0.2Al) and z = 3.4 in sample Amp(0.3Al) and 15R is also observed in these samples. Contrary to what was observed in samples formed from alpha silicon nitride, N:O ratio decreases in these phases as more Al is incorporated.

Fig. 5 displays the XRD patterns of samples containing α–Si$_3$N$_4$ sintered at 1450 °C. α–SiAlON is the major phase along with 21R polytypoid in α(0Al) and 12R in the samples containing Al metal. Also, SiO$_2$ is observed in sample α(0.3Al) as a minor phase [28–30]. β–SiAlON is not observed in these samples sintered at 1450 °C.

3.4. Microstructural development

FESEM micrographs of samples α(0Al), α(0.1Al), α(0.2Al) and α(0.3Al) sintered at 1600 °C are shown in Fig. 6. Sample α(0Al) is composed of two types of morphology: rod-like and equiaxed structures. XRD analysis has demonstrated that this sample consists of β-SiAlON with z = 3.2 and 15R polytypoid. It is known that β-SiAlON exhibits elongated morphology, which can be clearly observed in the FESEM image of Fig. 6a. β-SiAlON hexagonal grains,

showing their basal planes, can be seen in Fig. 6b. When Al metal is substituted for AlN, α-SiAlON (Ca$_{0.7}$Si$_{10}$Al$_2$O$_{0.7}$N$_{15.3}$) is formed in samples α(0.1Al), α(0.2Al) and α(0.3Al), whereas β-SiAlON is only present in sample α(0.1Al) (according to XRD and FESEM analyses). Several AlN polytypoid phases are observed in these samples. Figs. 6c and d reveal that the aspect ratio of SiAl$_5$O$_2$N$_5$ (12H) phase is lower than that of the SiAl$_6$O$_2$N$_6$ (21R) phase. Comparing Fig. 6a, which corresponds to sample α(0Al), with the remaining micrographs of lower magnification, it can be seen that the level of secondary polytypoid phase(s) dispersion is enhanced as Al metal replacement is increased.

The formation of elongated α-SiAlON grains occurs in sample α(0.3Al) sintered at 1600 °C, as shown in Fig. 6f. However, other samples have not shown this tendency. Kurama et al. [31] have reported that elongated α-SiAlON grains can be formed easily if α-SiAlON formation is hindered at low temperatures by using high heating rate sintering as in SPS. They also showed the necessity of having enough liquid phase, which occurs at high m and n values, to aid the elongation growth morphology that is thought to be diffusion-controlled [31]. However, Shen and Nygren [25] noted that the grains grow so fast during the SPS process, that diffusion controlled grain growth mechanisms proposed for traditional liquid-sintering do not fit with their observations and grain-coarsening seems to be controlled more by interface reactions.

FESEM micrographs of the samples produced from amorphous silicon nitride are shown in Fig. 7. β-SiAlON was the major phase in all the samples with the maximum amount observed in sample Amp(0.3Al). Various AlN polytypoid phases, mainly 15R (SiAl$_4$O$_2$N$_4$), are present also. α-SiAlON forms only in sample Amp(0.1Al), as shown in Fig. 7b and c. As Al replaces AlN, more β-SiAlON is formed at the expense of other phases with the amount of 15R reduced in sample Amp(0.3Al) (Fig. 7e) when compared with sample Amp(0.2Al) (Fig. 7d), which is also confirmed by XRD results shown in Fig. 4.

FESEM micrographs of samples containing α-Si$_3$N$_4$ sintered at 1450 °C are shown in Fig. 8. It was found that as the amount of Al increases the formation of α-SiAlON is restrained and 12H polytypoid is formed instead. A similar trend was identified from the XRD data (Fig. 5).

3.5. Role of precursors in phase formation

During sintering of silicon nitride and SiAlONs, liquid phase densification occurs. In general terms, initially the precursors react with silicon nitride and silica present on the nitride particle surfaces to form a Ca-Si-Al-O-N liquid phase above the eutectic temperature which is known to be at ~1250 °C. This promotes densification firstly through a particle rearrangement stage and secondly by a solution-diffusion-precipitation process in which the initial α-Si$_3$N$_4$ is dissolved in the liquid and transforms to α- or β-SiAlON along with formation of the AlN polytypoids.

A pure -SiAlON composition is nitrogen-rich and the volume of oxynitride liquid available for densification is low and of high viscosity. As -SiAlON is precipitated, the amount of liquid gradually reduces. This means that complete reaction to form the solid solution does not occur and some unreacted components or residual glass are normally present after sintering. Thus, the composition needs to be tailored to make it more oxygen rich as in the case of
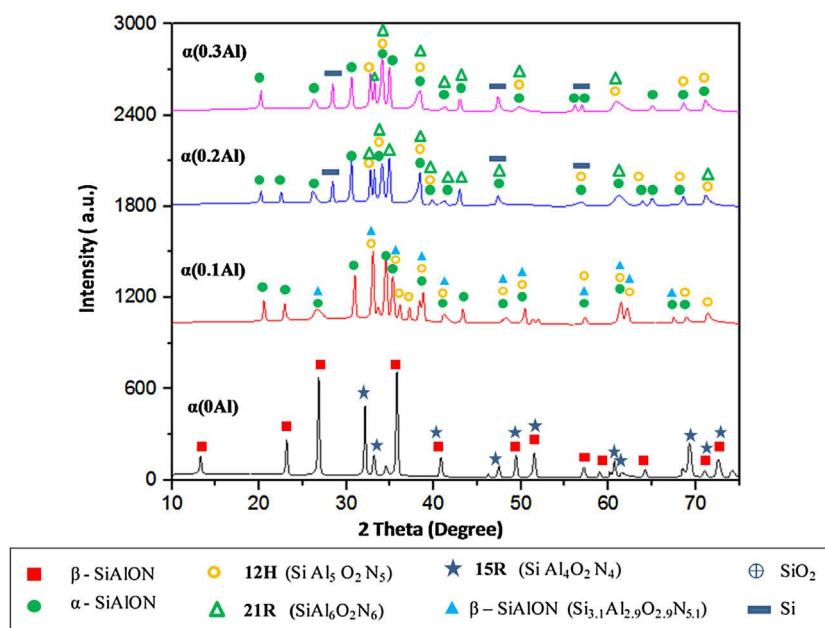
Fig. 3. XRD patterns of samples **α(0Al)**, **α(0.1Al)**, **α(0.2Al)** and **α(0.3Al)** samples, sintered at 1600 °C.
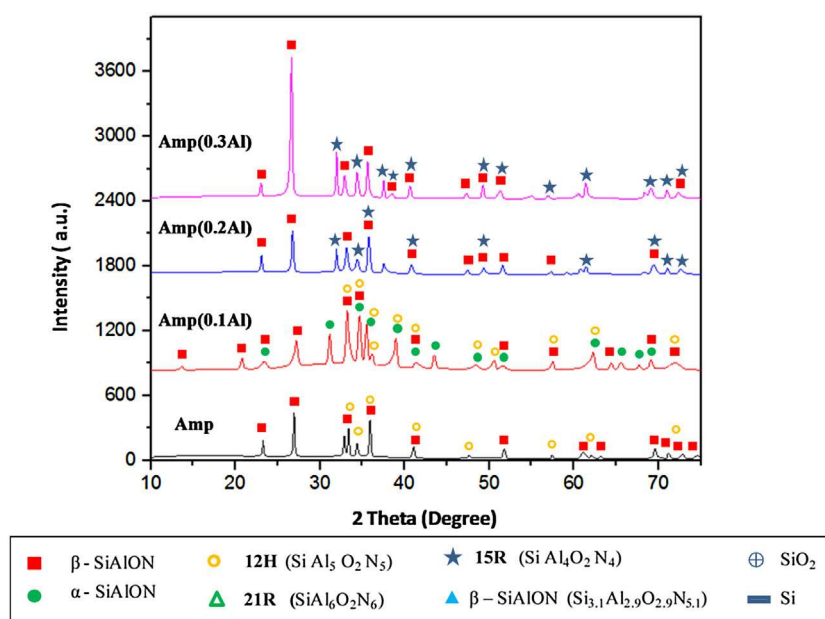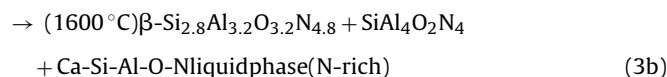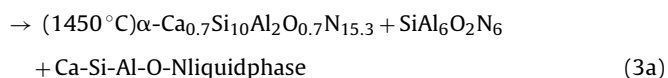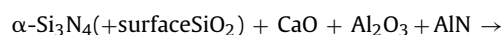

Fig. 4. XRD patterns of Amp, Amp(0.1Al), Amp(0.2Al) and Amp(0.3Al) samples, sintered at 1600 °C.

the composition used in this work, $CaSi_6Al_6O_4N_{12}$, so that more liquid is formed, facilitating densification but inevitably resulting in residual grain boundary crystalline or vitreous phases. As the overall composition is more Al- and O-rich than for a pure -SiAlON, this allows the formation of more liquid phase.

So for sample **α(0Al)**, using α-Si_3N_4 as precursor, based on XRD and the microstructural observations, the overall reaction can be shown schematically as:

$$\alpha\text{-}Si_3N_4(+surfaceSiO_2) + CaO + Al_2O_3 + AlN \rightarrow$$

$$\rightarrow (1450\,°C)\alpha\text{-}Ca_{0.7}Si_{10}Al_2O_{0.7}N_{15.3} + SiAl_6O_2N_6$$

$$+ Ca\text{-}Si\text{-}Al\text{-}O\text{-}N liquidphase \qquad (3a)$$

$$\rightarrow (1600\,°C)\beta\text{-}Si_{2.8}Al_{3.2}O_{3.2}N_{4.8} + SiAl_4O_2N_4$$

$$+ Ca\text{-}Si\text{-}Al\text{-}O\text{-}N liquidphase(N\text{-}rich) \qquad (3b)$$

Thus it appears that following rapid heating in the SPS equipment to 1450 °C, a large amount of an oxygen-rich Ca-SiAlON liquid is formed from which two N-rich crystalline phases, α-$Ca_{0.7}Si_{10}Al_2O_{0.7}N_{15.3}$ and 21R ($SiAl_6O_2N_6$) are formed. At higher temperature, the oxygen rich liquid phase reacts further with the -SiAlON to transform it to β-$Si_{2.8}Al_{3.2}O_{3.2}N_{4.8}$ leaving the liquid phase more N-rich. This has been observed previously by many
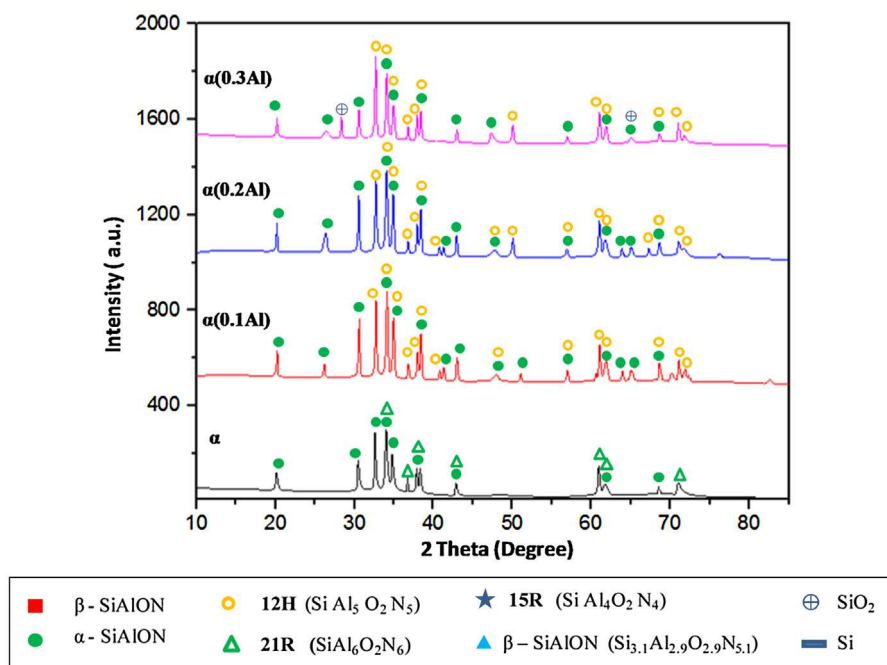
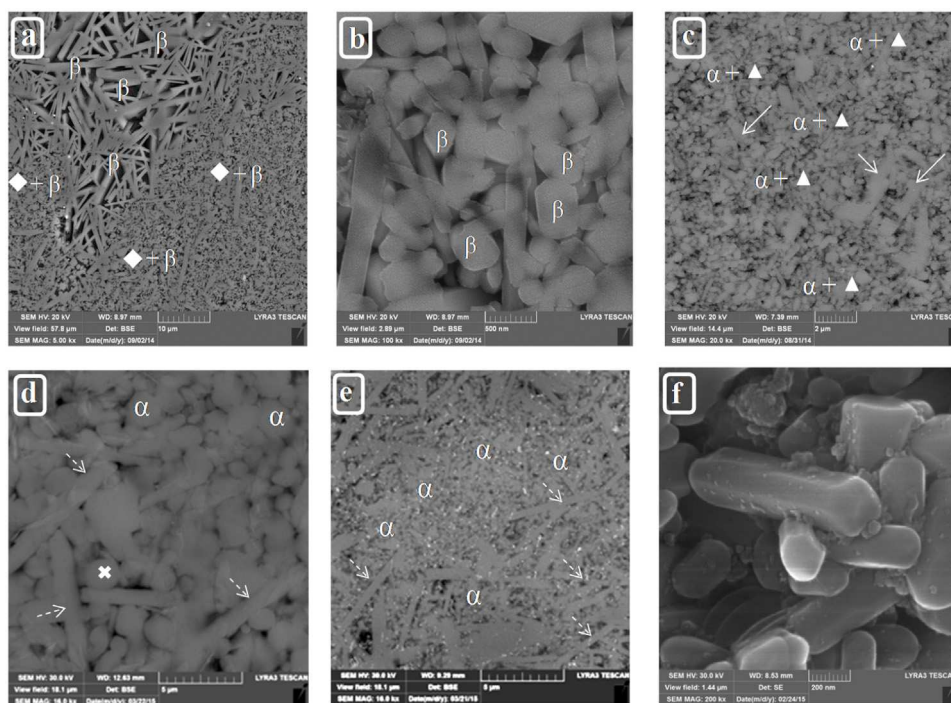Fig. 5. XRD patterns of **α(0Al)**, **α(0.1Al)**, **α(0.2Al)** and **α(0.3Al)** samples, sintered at 1450 °C.

Fig. 6. FESEM micrographs of samples containing α-Si$_3$N$_4$ sintered at 1600 °C. (a), (b) **α(0Al)**, (c) **α (0.1Al)**, (d) **α (0.2Al)**, (e) **α (0.3Al)**, (f) a fracture surface of **α (0.3Al)**. Label key: β-SiAlON z = 3.2 (β), α-SiAlON (α), β-SiAlON z = 2.9 (▲), 12R (→), 21R (—►), SiO$_2$ (**x**).

researchers [3,10,17,32]. The liquid cools to form a grain boundary glass.

For the samples containing Al in place of some of the AlN, the overall reaction at both temperatures can be shown as:

$$\alpha\text{-Si}_3N_4(+\text{surface SiO}_2) + CaO + Al_2O_3 + AlN + Al + N_2 \rightarrow$$

$$\rightarrow \alpha\text{-Ca}_{0.7}Si_{10}Al_2O_{0.7}N_{15.3} + SiAl_6O_2N_6$$
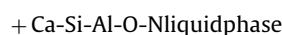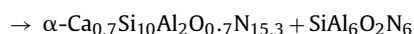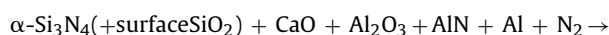
$$+ \text{Ca-Si-Al-O-N liquid phase} \qquad (4)$$

Al melts at 660 °C and nitridation of Al occurs above ∼800 °C [33]. In SPS with rapid heating, the nitridation reaction would occur over a range of temperatures. Eventually, the Ca-SiAlON liquid is formed from which the two N-rich crystalline phases, α-Ca$_{0.7}$Si$_{10}$Al$_2$O$_{0.7}$N$_{15.3}$ and 21R are observed at both 1450 °C and 1600 °C. This is due to the fact that the presence of Al favours the formation of a more N-rich liquid phase at 1450 °C and therefore there is no further reaction and transformation at higher temperatures to form β-SiAlON.
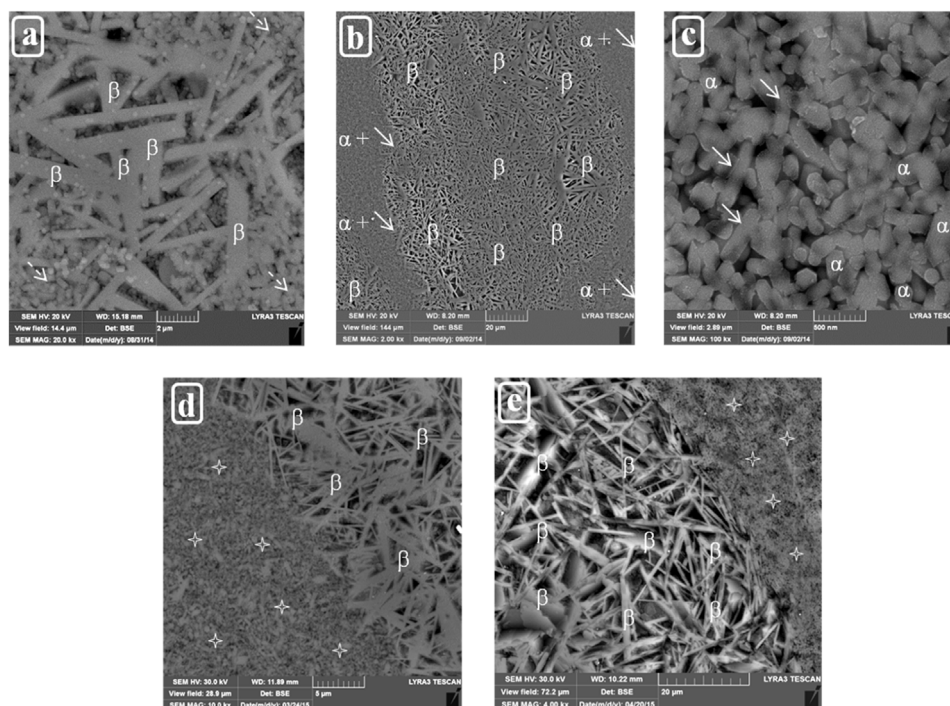
Fig. 7. FESEM micrographs of samples containing amorphous-Si_3N_4 sintered at 1600 °C. (a) **Amp(0Al)**, (b), (c) **Amp(0.1Al)**, (d) **Amp(0.2Al)**, (e) **Amp(0.3Al)**. **Label key:** β-SiAlON (β), α-SiAlON (α), 15R (+), 12H (→), 21R (—▶).
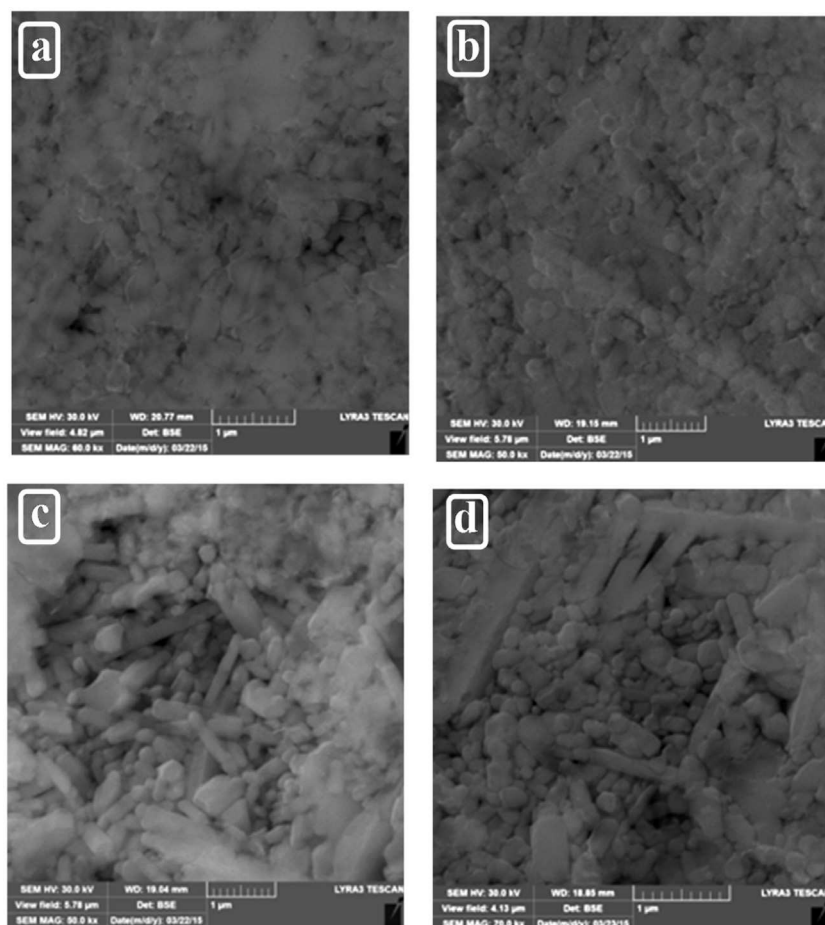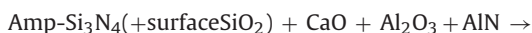

Fig. 8. FESEM micrographs of samples containing α-Si_3N_4 sintered at 1450 °C. (a) **α(0Al)**, (b) **α(0.1Al)**, (c) **α(0.2Al)**, (d) **α(0.3Al)**.

Table 3
Experimental results of the samples sintered at 1450 °C and 1600 °C.

Sample Name	After sintering at 1450 °C		After sintering at 1600 °C	
	HV_{10} [GPa]	K_{IC} [MPa$\sqrt{m}$]	HV_{10} [GPa]	K_{IC} [MPa$\sqrt{m}$]
α(0Al)	17.0 ± 0.3	4.4 ± 0.8	13.4 ± 0.7	7.2 ± 2.4
α(0.1Al)	18.6 ± 0.4	7.8 ± 0.8	13.7 ± 0.6	6.4 ± 1.5
α(0.2Al)	19.1 ± 0.2	6.4 ± 0.4	16.0 ± 0.5	9.5 ± 1.9
α(0.3Al)	19.6 ± 0.3	6.5 ± 0.8	18.5 ± 0.7	8.3 ± 0.7
Amp(0Al)	–	–	12.3 ± 0.8	5.2 ± 1.3
Amp(0.1Al)	–	–	12.2 ± 0.3	6.1 ± 1.5
Amp(0.2Al)	–	–	13.3 ± 0.4	5.3 ± 1.0
Amp(0.3Al)	–	–	14.4. ± 1.0	–

In the case of the samples based on using amorphous silicon nitride, for **Amp(0Al),** with no Al substituted for AlN, the reaction schematic is as follows:

$$Amp\text{-}Si_3N_4(+surface SiO_2) + CaO + Al_2O_3 + AlN \rightarrow$$

$$\rightarrow \beta\text{-}Si_{4.8}Al_{1.2}O_{1.2}N_{6.8} + SiAl_5O_2N_5 + Ca\text{-}Si\text{-}Al\text{-}O\text{-}N\, liquid\, phase \quad (5)$$

So in this sample, β-SiAlON with z = 1.2 is formed at the expense of α-SiAlON even at 1600 °C. Thus it would appear that, following rapid heating in the SPS equipment, a large amount of an oxygen-rich Ca-SiAlON liquid is formed from which $\beta\text{-}Si_{4.8}Al_{1.2}O_{1.2}N_{6.8}$ is precipitated along with 12H. As the amorphous Si_3N_4 is an extremely fine powder (20 nm), then the amount of silica on its surface will be much more than in the case of the α-Si₃N₄ (250 nm) and therefore the overall composition will be more oxygen rich leading to precipitation of β-SiAlON.

As Al is substituted for AlN in these samples, β-SiAlON with much higher z value is still the major phase with 15R polytypoid as a minor phase according to the following schematic:

$$Amp\text{-}Si_3N_4(+surface SiO_2) + CaO + Al_2O_3 + AlN + Al + N_2 \rightarrow$$

$$\rightarrow \beta\text{-}Si_{2.6}Al_{3.4}O_{3.4}N_{4.6} + SiAl_4O_2N_4 + Ca\text{-}Si\text{-}Al\text{-}O\text{-}N\, liquid\, phase \quad (6)$$

It is clear that, since β-SiAlON is the major phase, the overall composition must be more oxygen rich due to the excess surface silica on this type of silicon nitride. Even in the **Amp(0.3Al)** composition, some crystalline SiO_2 is observed in the final phase assemblage.

From the sintering results it is clear that there is very little difference between the densities of the different groups of samples, thus indicating that in all cases a sufficient amount of liquid phase was formed which allowed full densification. However, there were obvious differences between the compositions of the liquid phases formed which affected the subsequent reactions and transformations and final phase assemblages.

3.6. Mechanical properties

Table 3 shows mechanical properties of samples sintered at 1450 and 1600 °C.

Hardness values for samples using α-Si₃N₄ sintered at 1450 °C were in the range 17.0–19.6 GPa, increasing with substitution of Al for AlN. On sintering at 1600 °C, there is a significant decrease in hardness for samples α(0Al) and α(0.1Al). This is clearly due to the differences in phase assemblages as these samples contain β-SiAlON in place of Ca-α-SiAlON. α-SiAlON is known to be intrinsically harder than β-SiAlON. For this reason, the low hardness values in the range 12.3–14.4 GPa measured for the samples using amorphous-Si₃N₄ sintered at 1600 °C are due to the fact that in these samples, only β-SiAlON and AlN polytypoids and glass phase are present. In summary, hardness values can be clearly related to the particular phases present in the microstructures and increases

are observed in both sets of compositions sintered at 1450 and 1600 °C as Al is substituted for AlN.

For samples using α-Si₃N₄ sintered at 1450 °C, fracture toughness is 4.4 MPa√m for the α(0Al) and increases to values in the range 6.4–7.8 MPa√m when Al is substituted for AlN. After sintering at 1600 °C, the fracture toughness increases for most compositions to values in the range 6.4–9.5 MPa√m but there are wide variations in standard deviations for samples α(0Al), α(0.1Al) and α(0.2Al). Sample α(0.3Al) has a fracture toughness of 8.3 ± 0.7 MPa√m and this is the sample which exhibits α-SiAlON with high aspect ratio elongated grains. This, combined with a hardness of 18.5 GPa, suggests that this composition containing α-Si₃N₄ as a precursor along with 30 mol% substitution of Al in AlN by Al metal sintered by SPS has promising mechanical properties that should be explored further.

4. Conclusions

Densification by spark plasma sintering (SPS) in a nitrogen environment and mechanical properties of a fixed Ca-α-SiAlON composition, to allow excess liquid formation, using different nano- and sub-micron precursors were investigated. These were α-Si₃N₄ (250 nm), amorphous-Si₃N₄ (20 nm) and AlN with substitution of 0, 10, 20, and 30 mol% of Al metal.

SPS processing was performed firstly at 1600 °C at which all densities are close to 3.1 g cm⁻³. Further, samples sintered at 1450 °C had the same or higher densities suggesting that, by using SPS with its inherent rapid heating rate and the associated uniaxial pressure, densification can be achieved very easily even at lower peak temperatures.

At 1450 °C, Ca-α-SiAlON and polytypoids are formed along with an oxygen-rich Ca-SiAlON liquid phase. At 1600 °C, this liquid reacts further with -SiAlON to transform it to β-SiAlON. When Al is substituted for AlN, Ca-α-SiAlON and 21R are observed at both temperatures. The presence of Al favours the formation of a more N-rich liquid phase at 1450 °C and therefore, there is no further reaction and transformation at higher temperatures to form β-SiAlON.

Increases in Vickers hardness are observed in both sets of compositions sintered at 1450 °C and 1600 °C as Al is substituted for AlN. After sintering at 1600 °C, fracture toughness ranges from 5 to 9 MPa√m depending on composition. The composition containing α-Si₃N₄ as a precursor along with 30 mol% substitution of Al metal sintered by SPS has a fracture toughness of 8.3 MPa√m and hardness of 18.5 GPa and with these promising mechanical properties this composition should be explored further.

Acknowledgment

References

[1] K.H. Jack, W.I. Wilson, Ceramics based on the Si-Al-ON and related systems, Nature 238 (80) (1972) 28–29.
[2] S. Hampshire, H.K. Park, D.P. Thompson, K.H. Jack, α′-Sialon ceramics, Nature 274 (5674) (1978) 880–882.
[3] G.Z. Cao, Ruud Metselaar, Alpha. '-sialon ceramics: a review, Chem. Mater. 3 (2) (1991) 242–252.
[4] K.H. Jack, Sialons and related nitrogen ceramics, J. Mater. Sci. 11 (6) (1976) 1135–1158.
[5] Yoichi Oyama, Osami Kamigaito, Solid solubility of some oxides in Si3N4, Jpn. J. Appl. Phys. 10 (11) (1971) 1637.

[6] Y. Zhou, Jozef Vleugels, Tahar Laoui, Petar Ratchev, Omer Van der Biest, Preparation and properties of X-sialon, J. Mater. Sci. 30 (18) (1995) 4584–4590.

[7] J. Leugels, T. Laoui, M. Wouters, O. Van der Biest, Characterization of sialon ceramics by EPMA and TEM, Institute of Physics Conference Series (1993).

[8] Tahar Laoui, Omer Van der Biest, Study of grain boundary phase in silicon nitride materials by Raman spectroscopy, Key Eng. Mater. 89–91 (1993) 495–500.

[9] V.A. Izhevskiy, L.A. Genova, J.C. Bressiani, F. Aldinger, Progress in sialon ceramics, J. Eur. Ceram. Soc. 20 (13) (2000) 2275–2295.

[10] Thommy Ekström, Mats Nygren, SiAlON ceramics, J. Am. Ceram. Soc. 75 (1992).

[11] I.H. Shin, J. Kim Deug, Growth of elongated grains in α -sialon ceramics, Mater. Lett. 47 (6) (2001) 329–333.

[12] I.-Wei Chen, Anatoly Rosenflanz, A tough sialon ceramic based on A-Si3N4 with a whisker-like microstructure, Nature 389 (6652) (1997) 701–704.

[13] Mathias Herrmann, Sören Höhn, Axel Bales, Kinetics of rare earth incorporation and its role in densification and microstructure formation of α-sialon, J. Eur. Ceram. Soc. 32 (7) (2012) 1313–1319.

[14] Yvonne Menke, Valerie Peltier-Baron, Stuart Hampshire, Effect of rare-earth cations on properties of sialon glasses, J. Non-Cryst. Solids 276 (1) (2000) 145–150.

[15] Siddhartha Bandyopadhyay, M.J. Hoffmann, G. Petzow, Effect of different rare earth cations on the densification behaviour of oxygen rich A-sialon composition, Ceram. Int. 25 (3) (1999) 207–213.

[16] Abbas Saeed Hakeem, Jekabs Grins, Saeid Esmaeilzadeh, La–Si–O–N glasses: part I. Extension of the glass forming region, J. Eur. Ceram. Soc. 27 (16) (2007) 4773–4781.

[17] G.Z. Cao, Ruud Metselaar, G. Ziegler, Relations between composition and microstructure of sialons, J. Eur. Ceram. Soc. 11 (2) (1993) 115–122.

[18] P.L. Wang, C. Zhang, W.Y. Sun, D.S. Yan, Formation behavior of multi-cation A-sialons containing calcium and magnesium, Mater. Lett. 38 (3) (1999) 178–185.

[19] P.L. Wang, Y.W. Li, D.S. Yan, Effect of dual elements (Ca, Mg) and (Ca, La) on cell dimensions of multi-cation A-sialons, J. Eur. Ceram. Soc. 20 (9) (2000) 1333–1337.

[20] Raja Muhammad Awais Khan, Moath Mohammad Al Malki, Abbas Saeed Hakeem, Muhammad Ali Ehsan, Tahar Laoui, Development of a single-phase Ca- α -sialon ceramic from nanosized precursors using spark plasma sintering, Mater. Sci. Eng.: A 673 (2016) 243–249.

[21] J.W.T. Van Rutten, H.T. Hintzen, Ruud Metselaar, Densification behaviour of Ca-A-sialons, Ceram. Int. 27 (4) (2001) 461–466.

[22] Limeng Liu, Feng Ye, Yu Zhou, Zhiguo Zhang, Qinglong Hou, Fast bonding A-sialon ceramics by spark plasma sintering, J. Eur. Ceram. Soc. 30 (12) (2010) 2683–2689.

[23] M. Belmonte, J. González-Julián, P. Miranzo, M.I. Osendi, Spark plasma sintering: a powerful tool to develop new silicon nitride-based materials, J. Eur. Ceram. Soc. 30 (14) (2010) 2937–2946.

[24] David Salamon, Zhijian Shen, Pavol Šajgalík, Rapid formation of A-sialon during spark plasma sintering: its origin and implications, J. Eur. Ceram. Soc. 27 (6) (2007) 2541–2547.

[25] Zhijian Shen, M. Nygren, Kinetic aspects of superfast consolidation of silicon nitride based ceramics by spark plasma sintering, J. Mater. Chem. 11 (1) (2001) 204–207.

[26] Abbas S. Hakeem, Rachel Daucé, Ekaterina Leonova, Mattias Edén, Zhijian Shen, Jekabs Grins, Saeid Esmaeilzadeh, Silicate glasses with unprecedented high nitrogen and electropositive metal contents obtained by using metals as precursors, Adv. Mater. 17 (18) (2005) 2214–2216.

[27] A.G. Evans, E.A. Earn, Fracture toughness determinations by indentation, J. Am. Ceram. Soc. 59 (7–8) (1976) 371–372.

[28] K.H. Jack, The characterization of A'-sialons and the A–B relationships in sialons and silicon nitrides, in: Progress in Nitrogen Ceramics, Springer, 1983, pp. 45–60.

[29] S. Wild, P. Grieveson, K.H. Jack, The crystal structure of alpha and beta silicon and germanium nitrides, Spec. Ceram. 5 (1972) 385–395.

[30] H.F. Priest, F.C. Burns, G.L. Priest, E.C. Skaar, Oxygen content of alpha silicon nitride, J. Am. Ceram. Soc. 56 (7) (1973) 395.

[31] S. Kurama, M. Herrmann, H. Mandal, The effect of processing conditions, amount of additives and composition on the microstructures and mechanical properties of A-sialon ceramics, J. Eur. Ceram. Soc. 22 (1) (2002) 109–119.

[32] Mandal Hasan, New developments in A-sialon ceramics, J. Eur. Ceram. Soc. 19 (13) (1999) 2349–2357.

[33] Patama Visuttipitukul, Tatsuhiko Aizawa, Hideyuki Kuwahara, Advanced plasma nitriding for aluminum and aluminum alloys, Mater. Trans. 44 (12) (2003) 2695–2700.